Available online at www.sciencedirect.com
ScienceDirect
International Journal of Multiphase Flow 33 (2007) 448–468
International Journal of Multiphase Flow
www.elsevier.com/locate/ijmulflow

Pendant drop thread dynamics of particle-laden liquids

Roy J. Furbank [a,1], Jeffrey F. Morris [b,*]

[a] School of Chemical and Biomolecular Engineering, Georgia Institute of Technology, Atlanta, GA 30332, United States
[b] The Benjamin Levich Institute and Department of Chemical Engineering, City College of New York, New York, NY 10031, United States

Received 18 March 2005; received in revised form 27 February 2006

Abstract

Temporal evolution of pendant drops toward pinch-off is studied for a particle-laden liquid. Stretching and thinning of the necking region, or thread, are quantified for suspensions of monodisperse noncolloidal particles over a range of particle volume fractions, ϕ. The stretching is characterized by the length of connected material attached to the orifice as this evolves from the quasistatic drop to bifurcation. Drop formation from suspensions of $0 \leqslant \phi \leqslant 0.4$ was studied and compared with the same process for liquids of varying viscosity but the same surface tension as the suspension. Two orifice sizes and two noncolloidal particle sizes, at ratios of orifice to particle diameter of 12.8 and 25.6, were studied at tube-scale Reynolds numbers of $Re = 10^{-2}$, capillary numbers of $Ca < 0.1$ and Bond numbers of $0.5 < Bo < 2.5$. At large times prior to thread rupture, the added viscosity imparted to the mixture by the particles causes a slower thinning than is observed for the pure liquid. As rupture is approached, thinning at the narrowest part of the thread is more rapid for suspensions than for pure liquid. More viscous pure liquids result in longer thread length at rupture, while the presence of particles, even at small ϕ, results in shorter connected length at rupture. These observations support a two-stage description of the drop formation process from suspensions. The first stage (far in time from rupture) is described well by a continuum representation of the particle phase resulting in an empirical increased effective shear viscosity, while the second stage (near in time to rupture) requires consideration of the finite-sized and discrete particles. The second stage evolution involves a localized thinning of the thread through a short axial span of dilute or particle-free material, and this localization results in the more rapid thinning and shorter thread lengths at rupture in the suspensions. A clear delineation in time between the first and second stages has not been identified.

1. Introduction

In this work, the role of particles in drop formation is examined. We study slow pendant drop formation for a neutrally buoyant suspension flowing from a circular orifice, focusing on the influence of the particles on the dynamics of the thread connecting the forming drop with the material remaining attached to the orifice after thread rupture. This is a suspension flow with a free surface, and such flows have received little study. The motivations for such study include such applications as suspension coating of paper and ink-jet

* Corresponding author.
E-mail address: jmorris@che.ccny.cuny.edu (J.F. Morris).
[1] Present address: Rohm and Haas Company, Spring House Technical Center, Spring House, PA 19477, United States.

0301-9322/$ - see front matter © 2006 Elsevier Ltd. All rights reserved.
doi:10.1016/j.ijmultiphaseflow.2006.02.021

application of particles in a carrier fluid. In natural settings, particle motions in free surface flows occur under dilute conditions in mucoid layers and the liquid layers in the lungs, and under concentrated conditions in mud flows. From a fundamental perspective, the interaction of a suspension, an assembly of particles, with a surface having interfacial tension introduces forces to the system which may lead to new phenomena. Distortion of a free surface may drive instabilities in certain circumstances, including that of a fluid column undergoing axial stretching, where the varicose or capillary instability is well-known. The presence of particles in such a column will generally result in such deformations under flow conditions, and thus may be expected to alter the characteristics of drop formation. While its characteristics may differ under different conditions, any drop formation process in axisymmetric geometry is expected to exhibit a thin extending column of fluid as the system progresses toward rupture. We seek to develop general understanding of particulate effects upon drop formation, and to this end we study here the slow drop formation with a focus upon particulate effects upon the dynamics of the stretching and thinning of the thread as the rupture is approached.

It is appealing to apply an effective single-phase fluid model to the behavior of suspensions. In such an approach, for a noncolloidal suspension the influence of the particles is accounted in simplest terms by an effective viscosity depending upon the solids volume fraction, ϕ. The expectation based upon the effective fluid approach is that adding particles will increase the viscosity, shifting the behavior from that of the suspending fluid to that of the pure liquid of viscosity the same as the effective viscosity of the mixture. Higher viscosity in pure liquids, as is well-known and also illustrated in experiments performed here for purposes of comparison, slows the rate of stretching and thinning throughout the drop-forming process and leads to an increase in the thread length at pinch-off. The influence of particles will be shown to agree with this behavior far in time from thread rupture, or what we will also term drop pinch-off, in slowing the stretching. However, the particles' effect will be seen to be in sharp contrast to the effective fluid prediction near in time to rupture. Specifically, near rupture, thinning is more rapid for the suspension and leads to shorter thread lengths at rupture.

1.1. Background

The area of drop formation is an area of research with an extensive history as well as much current interest. The most relevant body of literature to this work is the area of the formation of pendant drops of pure liquids since there has not been any work done of the formation of pendant drops of particle-laden liquids, as far as we have been able to discern.

Pure fluid pendant drop formation has been widely studied and the interested reader is referred to a review paper by Eggers (1997). The liquid thread which develops as the forming drop falls away from the orifice tip was apparently first studied in detail by Peregrine et al. (1990), who were able to capture this region using high-speed photography and elucidate the asymmetry of the structure formed just prior to the ultimate rupture, or bifurcation, of the liquid thread. Shi et al. (1994) examined the pinch-off structures formed for increasingly viscous liquids and determined that an increase in viscosity leads to longer threads at pinch-off. These authors also investigated pinch-off structures numerically using a set of one-dimensional equations developed by Eggers and Dupont (1994) and found that the numerical solutions agreed qualitatively with the experimental observations.

The dynamics of pure liquid pendant drop formation has been examined in a number of studies, e.g. those by Basaran and coworkers: Zhang and Basaran (1995), Wilkes et al. (1999), Ambravaneswaran et al. (2002) and Chen et al. (2002). Zhang and Basaran examined the dynamics of pendant drop formation experimentally and found that increasing viscosity led to longer thread lengths before pinch-off. Clanet and Lasheras (1999) also investigated the temporal evolution of pendant drops in the low-flow limit. They measured the thickness of the thinning thread as a function of time as pinch-off was approached and were successful in fitting the experimental measurements to an exponential decay model.

1.2. Motivation

These experiments were motivated by our previous work (Furbank and Morris, 2004) in which we examined the role of particles in the formation of pendant drops and the transition to slow jetting. There, in the case of the pendant drop, we observed that the necking process of the forming drop for the particle-laden cases

appeared to occur in two stages. In the initial stage of necking the thread that developed as the drop fell under the action of gravity was thicker for the suspensions examined than for the pure liquid, an effect which became more pronounced with increasing particle concentration. Initial necking continued until the thread had thinned sufficiently that the length scale of individual particles within the liquid became important. At this point the necking process changed and further thinning occurred in a more localized region devoid of particles. We termed this second stage "final necking" and hypothesized that it occurred in a similar fashion to that observed for pure liquids. Here, we describe a focused examination of the necking process alone, and at a higher resolution, with the aim of probing the validity of our proposed two-stage model for the necking of concentrated suspensions.

2. Experimental

Pendant drops of suspension were formed directly at the tip of a cylindrical capillary tube, with the orifice face electrolytically cut and flat (Valco Instruments). The orifice face was wetted to its outer diameter. The experimental set-up is illustrated schematically in Fig. 1. In the experiments, suspension was driven through a 3 cm long stainless steel capillary, with one of two outer (inner) radii of 0.16 (0.11) or 0.32 (0.22) cm, at low-flow rates using a syringe pump (Harvard Apparatus). Drops were imaged using a CCD camera (Kodak MotionCorder Analyzer, Model 1000) at a frame rate of 500 frames per second (fps). The chamber surrounding the drop generator, as shown in Fig. 1, was a glass box whose purpose was only to isolate the capillary from air currents in the laboratory. The entire apparatus was situated on a vibration-damped table (Newport).

2.1. Experimental details

The particles used were spherical poly (methyl methacrylate) (ICI Acrylics), in two particle size distributions (106–125 and 212–250 μm) obtained by manual sieving from the as-delivered material. The particles were suspended in a mixture of 23% (wt.) $ZnCl_2$ in H_2O solution and UCON 90000 (polyalkylene glycol; Dow Chemical). The composition of the suspending liquid was 70% (wt.) of the aqueous solution and 30% (wt.) UCON, with viscosity $\mu = 310 \pm 20$ cP at 25 °C, surface tension $\sigma = 49 \pm 3$ dyne/cm, and density of $\rho = 1.184 \pm 0.002$ g/cm^3. Density matching was sufficiently good that particles would remain suspended without appreciable settling or rising for one day.

These experiments focused on examining the low-flow behavior for a range of particle concentrations ϕ, for combinations of the two orifice sizes and two particle size distributions noted above. The conditions described in this study are listed in Table 1, where it is noted that the ratios of $d/d_p = 12.8$ and 25.6 were studied; experiments with the larger particles in the smaller orifice were not performed. The flow rate, Q, was fixed so that drops were formed very slowly (≈3.5 s between drops) with $Q = 0.25$ cm^3/min for the smaller orifice and

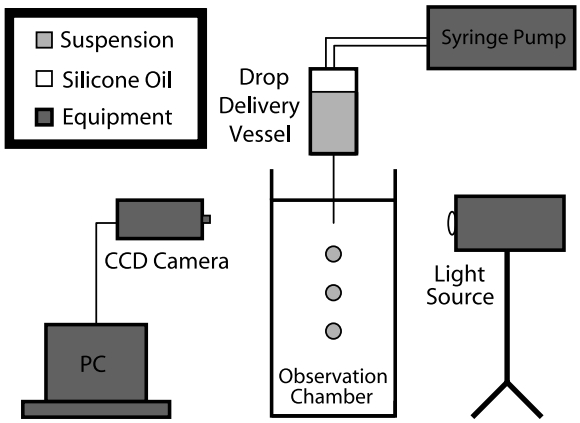

Fig. 1. Schematic of the experimental apparatus.

Table 1
Parameters for which experiments were performed

d (cm)	d_p (μm)	d/d_p	ϕ	Re	Ca	Bo
0.16	106–125	12.8	0–0.30	0.01	0.01	0.6
0.32	106–125	25.6	0–0.40	0.01	0.07	2.4
0.32	212–250	12.8	0–0.40	0.01	0.07	2.4

$Q = 0.50$ cm^3/min for the larger one so that $Re = \rho U d/\mu = 0.01$ throughout where $U = (4Q)/(\pi d^2)$ is the average velocity of the liquid through the capillary tube. In addition to the Reynolds number, drop formation in the absence of the particles is characterized by two other dimensionless measures: the capillary number, $Ca = \mu U/\sigma$, which characterizes the ratio of the viscous and surface forces and the Bond number, $Bo = \rho g d^2/\sigma$, the ratio of gravity to surface tension forces.

2.2. Typical experimental results

We have measured the rates of thinning and stretching of the thread connecting a forming drop of suspension to the material which remains at the orifice after rupture. In fact, the thread connecting the forming drop to the fluid which remains attached to the orifice after rupture is not unambiguously defined, and what was actually measured was the length of connected material from the orifice face to the end of the forming drop, L, and the minimum radius, R, of the thread. This data was obtained from digital photographic images and used to determine both the dimensionless thread length, $L(t)/d$, and dimensionless minimum thread radius, $R(t)/a$, as functions of time; the normalizing factors are the capillary diameter, d, and the particle radius, a, with the upper bound of each particle size distribution used (*i.e.* $2a = 125$ or 250 μm). The minimum thread radius at a given time was determined from the detected width profile of the forming drop, and was scaled by the particle radius in order to focus on the influence of the particle size as thinning progresses toward thread rupture. Fig. 2 shows typical L/d and R/a data for a suspension of $\phi = 0.10$ through an orifice of $d = 0.32$ cm with $d_p = 212$–250 μm. The photographs in Fig. 2 correspond to the times below which they appear.

We denote the time at which thread rupture occurs, *i.e.*, the instant of drop pinch-off, as t_0 and define this as the instant of the last image captured with an intact thread. The frame rate is 500 fps in all work presented here. In Fig. 2, L/d and R/a are plotted as functions of $t_0 - t$, or the time before rupture. The thread radius for the last three images (for which $t_0 - t \leqslant 0.004$ s) has fallen below the computer-aided detection limit, and thus the assessment of the last image with intact thread was performed by eye from the images. Our inability to measure the thread radius very near rupture is not considered of importance to consideration of the effects of noncolloidal particles since at times very near rupture the thread is composed of only liquid. It is therefore assumed to thin, and ultimately rupture, in the same manner as pure liquids. Primary interest here is in times relatively far from pinching yet well after necking has begun, as we seek to improve understanding of how the particles affect the process.

Note that the results described characterize only the necking process, a relatively short final portion of the drop formation process. The period between subsequent drops is long relative to the time over which necking occurs (typically more than an order of magnitude), with the majority of this time in the quasistatic growth condition during which stoppage of the flow would lead to a stable pendant drop (Furbank and Morris, 2004). Necking begins once the drop has attained a weight sufficient to exceed the force of surface tension acting along the contact line of the orifice edge. To illustrate this, we note that in the example of Fig. 2 the neck thins from a diameter near that of the orifice to rupture in 0.1 s, while the time between drops in this example is about 3.5 s.

3. Results

3.1. Necking behavior of suspensions

Results from the necking experiments are presented in both graphical form and as images representative of the process. For each d and d_p, we present measured L/d and R/a as well as a corresponding photographic

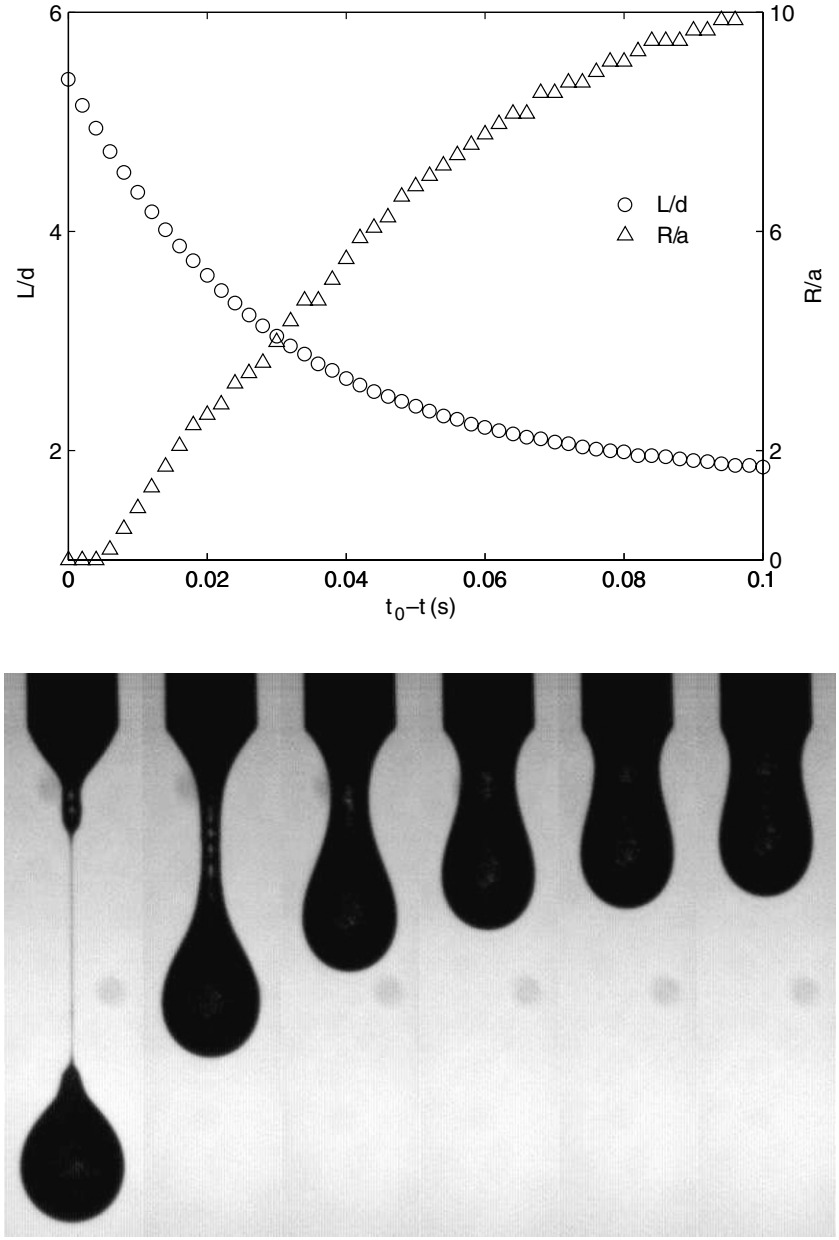

Fig. 2. Example of L/d and R/a as functions of time before rupture, $t_0 - t$, for $\phi = 0.10$, $d = 0.32$ cm, and $d_p = 212–250$ μm. The photographs correspond with the times below which they appear.

sequence of the process for different ϕ (see Figs. 3–6). Results from five separate drop formation events are shown in each data set. These curves provide a qualitative description of the necking behavior at a range of ϕ and provide some indication of particle-induced fluctuations.

3.1.1. Characteristics of thinning behavior in suspensions

In Fig. 3a and b, the L/d and R/a curves show results for the smaller of the two orifices, $d = 0.16$ cm. In (a) are results for the pure liquid, and in (b) the most concentrated suspension investigated for this orifice, $\phi = 0.30$ with $d_p = 106–125$ μm. The primary effect of the particles on L/d is to introduce increased variability as pinch-off is approached. The ultimate pinch-off length, however, is only mildly affected, with a small

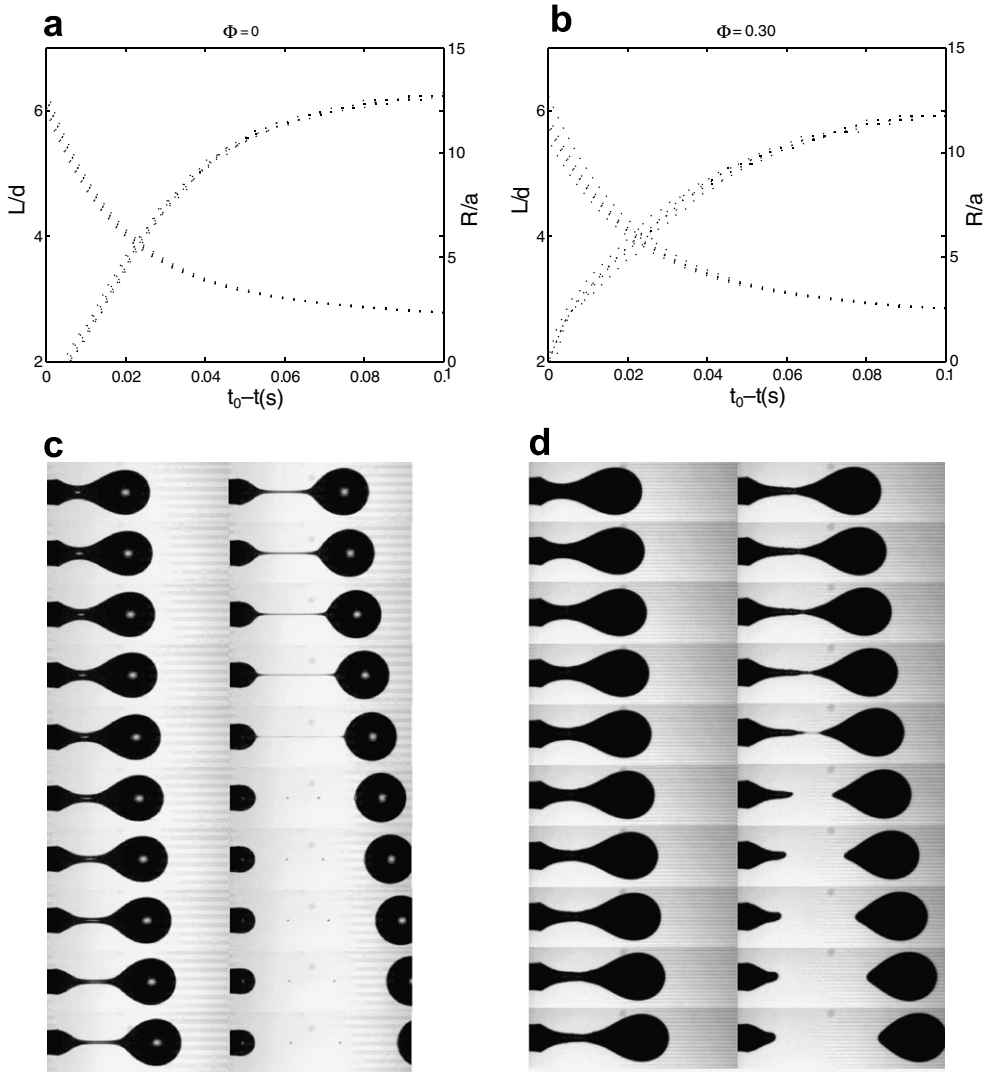

Fig. 3. L/d and R/a measurements for $\phi = 0$ (a) and $\phi = 0.30$ (b) with the corresponding photographic sequences, (c) and (d), for $d = 0.16$ cm, $d_p = 106$–125 μm. The time between images is (1/500) s and the last image captured before thread rupture is the 5th picture in the second column. This positioning is used throughout the remainder of the photographic sequences for ease of comparison.

decrease caused by the particles. The R/a data show more difference between the pure liquid and the concentrated suspension. Again, the addition of particles is observed to introduce increased fluctuations, and these become most pronounced at $t_0 - t \leqslant 0.04$ s. The suspension thread thins differently from the pure liquid at either end of the range of data displayed in the R/a curve. Near pinch-off, the slope of the R/a curve for the $\phi = 0.30$ suspension becomes progressively steeper (of larger $|\mathrm{d}R/\mathrm{d}t|$), in marked contrast to what is observed for the pure liquid, where the slope becomes weaker near t_0. For R/a at time far from pinch-off, the effect of the particles is to decrease the rate of thinning (smaller $|\mathrm{d}R/\mathrm{d}t|$), consistent with expectation based on the increased effective viscosity as shown quantitatively below in Section 3.3.

Fig. 3c and d presents photographic sequences for the conditions represented by the data of Fig. 3a and b, respectively. Images are shown for a short time before rupture ($t_0 - t \leqslant 0.028$ s) as well as for a short time after ($t_0 - t \geqslant -0.010$). As pinch-off is approached, the $\phi = 0.30$ suspension has a thicker neck than the pure liquid as shown by the bottom image in the left column from each condition (each taken at 0.01 s prior to rupture). The final thread thinning, and its eventual rupture, occurs for the suspension at a localized region

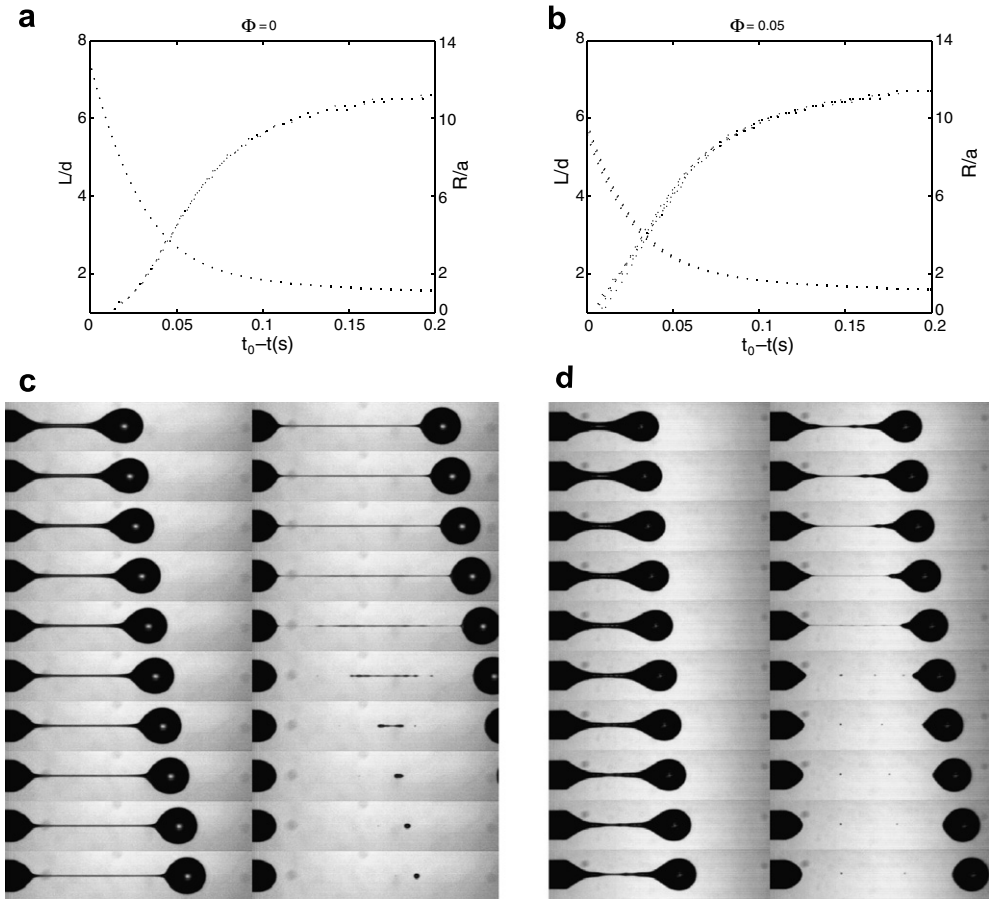

Fig. 4. L/d and R/a measurements for $\phi = 0$ (a) and $\phi = 0.05$ (b) with the corresponding photographic sequences, (c) and (d), for $d = 0.32$ cm, $d_p = 212$–250 μm. The time between images is (1/500) s.

along the length of the thread. This final necking rate is more rapid for the suspension, as shown in the R/a data for these two conditions. After rupture of the thread in the $\phi = 0.30$ case we see a behavior characteristic of the suspension, namely retraction of the large spindle structures, typically without formation of satellite drops (Furbank and Morris, 2004). This retraction following pinch-off often occurs asymmetrically, apparently reflecting variation in the particle distribution between the two spindle structures, thereby inducing some nonaxisymmetric (lateral) motion.

For the larger orifice diameter, $d = 0.32$ cm, results are presented in Figs. 4 and 5 with $d_p = 212$–250 μm for which $d/d_p = 12.8$ has the same value as used in the smaller orifice studies, and Fig. 6 with $d_p = 106$–125 μm for which $d/d_p = 25.6$. We observe similar trends in L/d and R/a to those seen in the smaller orifice with increasing ϕ, with a few notable exceptions.

In Fig. 4, the pure liquid is compared with a suspension of $\phi = 0.05$. For the pure liquid there is little drop-to-drop variability in either L/d or R/a. Once particles are present, even at the dilute fraction of $\phi = 0.05$, increased variation in the data is evident, and it is interesting to note observable steepening of $\mathrm{d}R/\mathrm{d}t$ near rupture. When compared with results from the smaller orifice, the particles lead to a larger decrease in L/d at pinch-off. This influence becomes stronger as ϕ is increased (Fig. 5), although the most pronounced effects are seen, from $L/d \approx 7.5$ to ≈ 5.8, for the initial addition of particles, *i.e.* from $\phi = 0$ to $\phi = 0.05$. At higher concentrations, $\phi = 0.20$ and 0.40 as shown in Fig. 5, the variability in both the thinning and stretching of the thread increases and the slope of the R/a curves becomes gradually steeper near, and flatter away from, pinch-off; both are similar to behaviors observed for the smaller capillary.

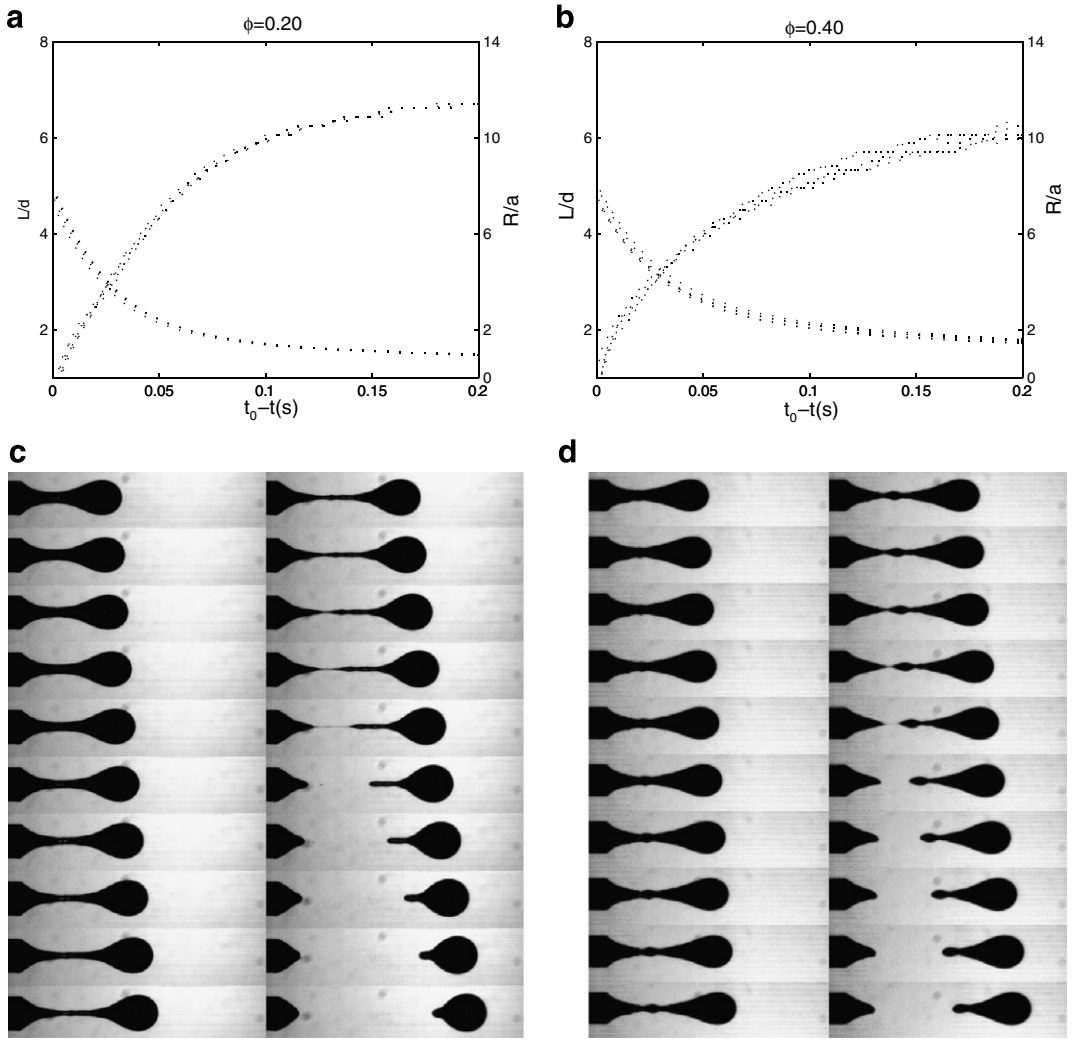

Fig. 5. L/d and R/a measurements for $\phi = 0.20$ (a) and $\phi = 0.40$ (b) with the corresponding photographic sequences, (c) and (d), for $d = 0.32$ cm, $d_p = 212$–250 μm. The time between images is (1/500) s.

These changes in the observed evolution with time of L/d and R/a with increasing ϕ are visually evident in the photographic sequences for the conditions presented in Fig. 4c and d for the pure liquid and low-ϕ suspension, and in Fig. 5c and d for $\phi = 0.2$ and $\phi = 0.4$. Increasing ϕ increases the size of the spindle structures formed near pinch-off, accompanied by a decrease in the length the thread attains before rupture.

Fig. 6 shows L/d and R/a for the $d = 0.32$ cm orifice with smaller particles, $d_p = 106$–125 μm, at solids loadings of $\phi = 0.10$ and 0.40. Both L/d and R/a show behavior similar to that of the larger particle suspensions for the same size orifice although the fluctuations at the highest ϕ are less pronounced. The photographic sequences for the smaller particles in Fig. 6c and d also show similar behavior to those for the larger particle suspensions although the thickness (R/a) of the spindle structures at moderate ϕ are smaller for the smaller particles. The asymmetric retraction of the up- and downstream spindle structures for the $\phi = 0.40$ suspension (Fig. 6d) is quite pronounced, a behavior also observed for the larger particle suspensions.

3.1.2. Average necking behavior

The average L/d and R/a for selected particle concentrations are shown for $d = 0.16$ cm with $d_p = 106$–125 μm in Fig. 7a and c, respectively, and for $d = 0.32$ cm with $d_p = 212$–250 μm in Fig. 7b and d, respectively. The average behavior allows a more direct comparison of the particulate effects on thinning and stretching of

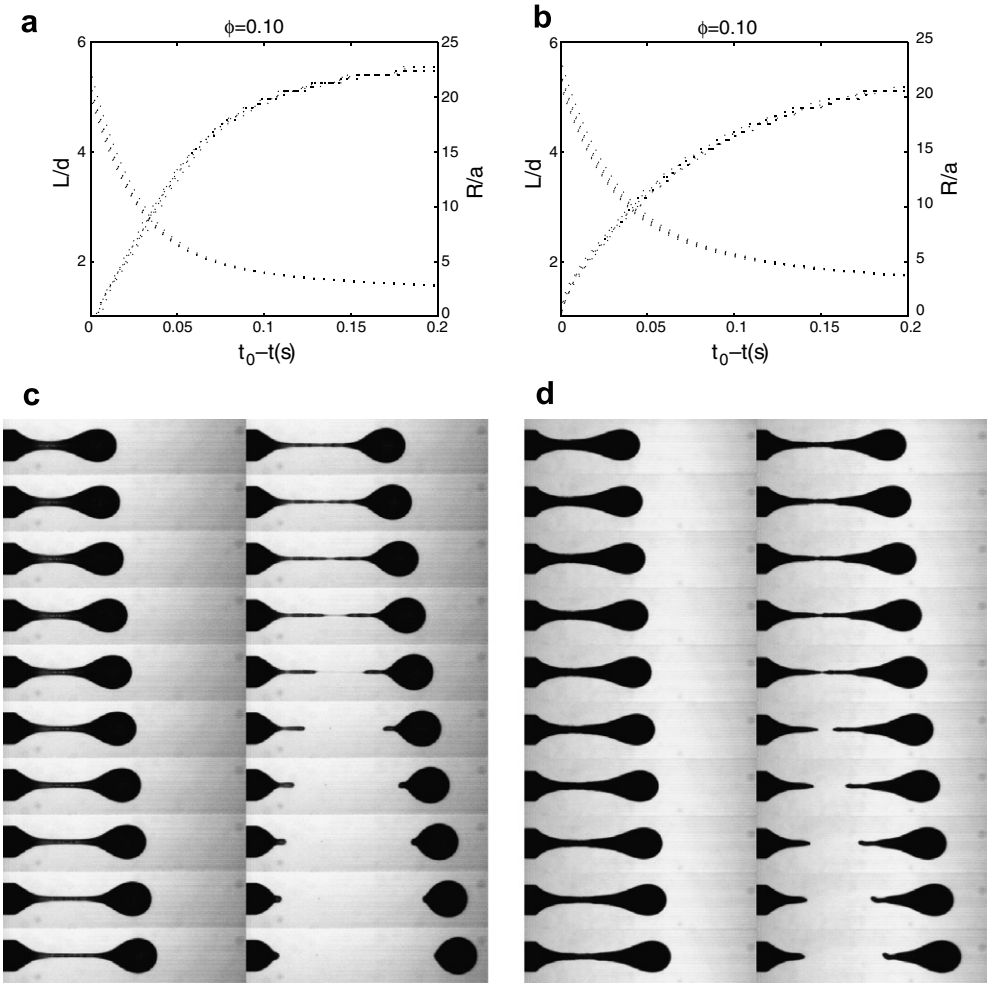

Fig. 6. L/d and R/a measurements for $\phi = 0.10$ (a) and $\phi = 0.40$ (b) with the corresponding photographic sequences, (c) and (d), for $d = 0.32$ cm, $d_p = 106$–125 μm. The time between images is (1/500) s.

the thread during necking. In these figures only data for the pure liquid, a low-ϕ and the largest-ϕ suspension studied are presented.

Fig. 7a and c presents the average $L(t)/d$ and $R(t)/a$, respectively, for the smaller orifice ($d = 0.16$ cm) at $\phi = 0$, 0.05, and 0.30. From the L/d data, it appears that the particles have little effect. At pinch-off both suspensions have a shorter length than the pure liquid but the effect is small, only about 6%. Away from pinch-off the L/d curves of the pure liquid and the $\phi = 0.05$ suspension are indistinguishable while the $\phi = 0.30$ suspension L/d data is slightly greater, possibly indicating an earlier onset of necking. The differences in R/a between the pure liquid and the suspensions are clearer for this smaller orifice. Far from pinch-off, the pure liquid and the $\phi = 0.05$ suspension are nearly identical while the $\phi = 0.30$ suspension is significantly thinner, implying a slower rate in this first stage of thinning. Near pinch-off, as noted in the previous section, the effect of the particles is to increase the slope of the R/a curve. For the pure liquid the thread thins more slowly as the time of rupture is approached, with the final necking occurring after the thread has thinned below the detection level possible here. The steepening of the thinning curve for the suspensions is observed even for the lowest-ϕ mixture examined for this orifice, $\phi = 0.05$, but becomes more pronounced at higher ϕ.

The average necking L/d and R/a data for the larger orifice, $d = 0.32$ cm, are presented in Fig. 7b and d, with trends similar to those seen in (a) and (c) for the smaller orifice but stronger particulate effects upon L at rupture. Experiments were also performed using the smaller particles ($d_p = 106$–125 μm) through this orifice

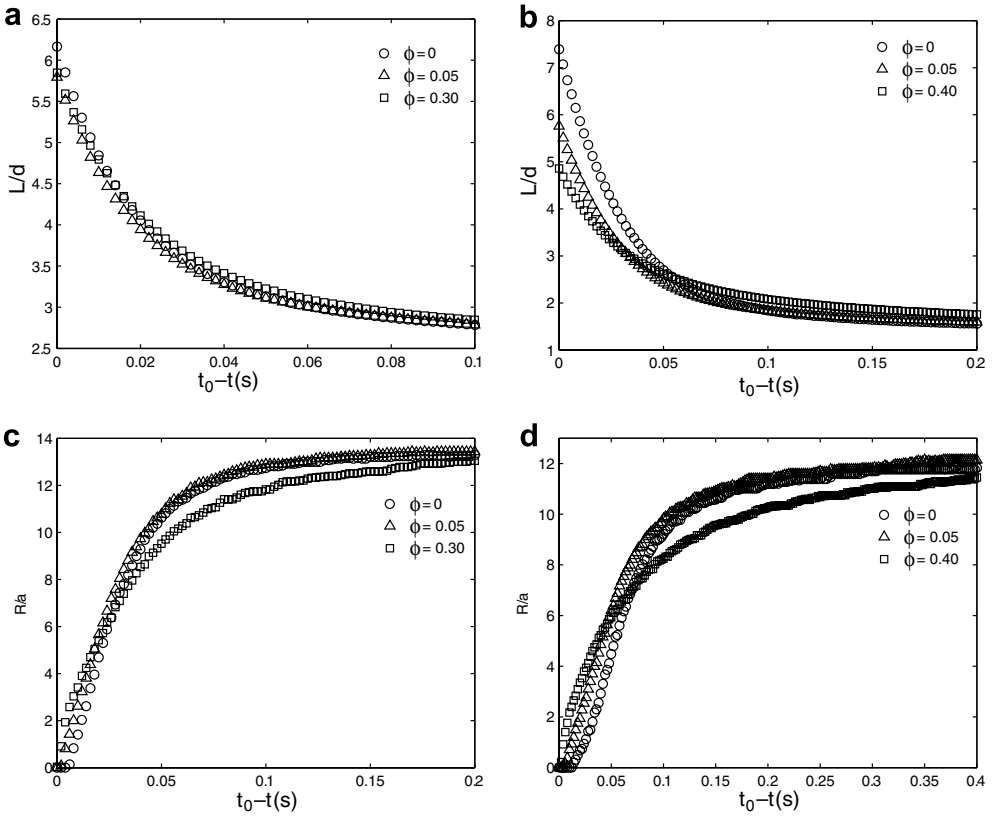

Fig. 7. Average L/d and R/a curves for $\phi = 0$, 0.05, and 0.30, $d = 0.16$ cm, $d_p = 106$–125 μm (a) and (c), and for $\phi = 0$, 0.05, and 0.40, $d = 0.32$ cm, $d_p = 212$–250 μm (b) and (d).

and the trends are again similar. The addition of particles causes a large decrease in the pinch-off length (~22%) in going from $\phi = 0$ to $\phi = 0.05$, with a continued but slower decrease as ϕ is raised. An increase in L/d at time far from pinch-off is also evident at the highest ϕ and is indicative of the particles increasing the overall necking times, as discussed previously for the smaller orifice. This lengthening of the necking interval is also seen in the thinning curves for $d = 0.32$ cm where the R/a values for $\phi = 0.40$ are less than those of the pure liquid or the low-ϕ suspensions at times relatively far from pinch-off. As pinch-off is approached, however, the curves cross implying that the trend is reversed: because time is measured from pinch and the necks of the concentrated suspensions are thicker, they thus must thin *more rapidly* than the pure liquid near the pinch.

3.2. Necking behavior of higher-viscosity pure liquids

Particles are well-known to increase the effective viscosity of a flowing mixture. In order to assess effective viscosity influence on the necking dynamics, two additional pure liquid samples were studied to provide a comparison. For ease of comparison, the liquids used consisted of the same three components as the suspending liquid ($ZnCl_2$, H_2O, UCON 90000) but with a greater percentage of UCON, the highly viscous component. The two additional samples prepared were a 35% UCON mixture ($\mu \doteq 520$ cP) and a 40% UCON mixture ($\mu \doteq 870$ cP). The suspending liquid was a 30% UCON mixture ($\mu \doteq 310$ cP). These two higher-viscosity liquids had surface tensions which were equal within the measurement accuracy to that of the suspending liquid of the suspensions. Results for drop formation from the higher-viscosity pure liquids and their comparison with the suspending liquid are presented in Fig. 8.

Fig. 8a and c shows L/d and R/a evolution for the three different viscosity mixtures through the smaller orifice ($d = 0.16$ cm). At a fixed volumetric flow rate, increasing viscosity causes a slowing of the necking,

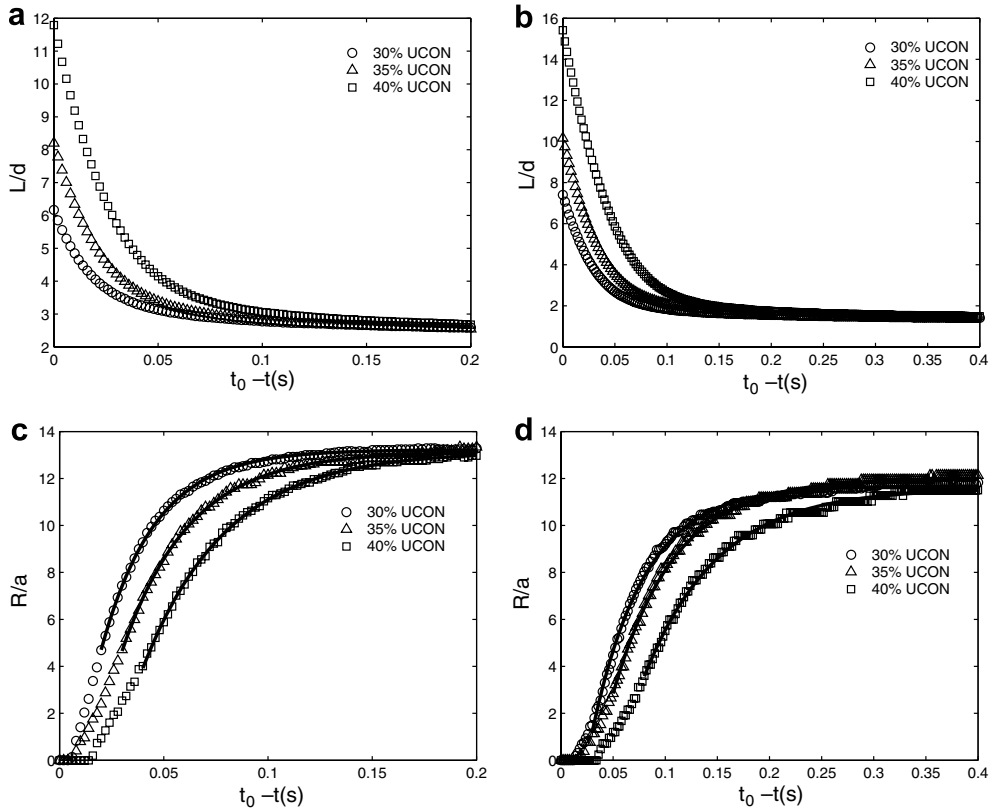

Fig. 8. Average L/d and R/a curves for the $d = 0.16$ cm orifice (a) and (c), and for the $d = 0.32$ cm orifice (b) and (d) for the varying viscosity pure liquids. The solid lines in the R/a plots, (c) and (d), represent the fit to model equation given in (1).

and leads to a large increase in the pinch-off length. For the $d = 0.16$ cm orifice the 40% UCON mixture has a pinch-off L/d of nearly twice that of the 30% UCON mixture. Since the necking time increases with increasing viscosity, thinning also begins earlier and slopes of the R/a curves over the entire time shown decrease with increasing viscosity.

The stretching and thinning curves for the various mixtures through the larger orifice ($d = 0.32$ cm) are shown in Fig. 8b and d. As for the smaller orifice, increasing the viscosity of the liquid leads to increases in the necking time with the corresponding increase in L/d and decrease in R/a at fixed times away from pinch-off.

We note several points regarding the influence of liquid viscosity on the necking dynamics and compare these effects to those of effective viscosity of suspensions presented in Section 3.1.2. The primary effect of increasing the viscosity of the pure liquid is to increase the resistance to stretching. This leads to slower thinning of the neck and longer necking times; a much longer thread length at pinch-off is also associated with the higher viscosity. Both similarities and differences are seen in comparing to results for the concentrated suspensions. The effect of increased overall necking time is common between higher-viscosity liquids and concentrated suspensions. This increase in the necking time for the suspensions can be seen in the variation with time of R/a away from thread rupture, where the thinning is slowed relative to the pure liquid, in a manner similar to that observed upon moving to the higher-viscosity liquid-only systems. As pinch-off is approached, however, the behaviors of the suspension and more viscous liquid-only cases are, in fact, quite different. Near pinch-off, thinning for the pure liquids occurs at slower rates for increasing viscosity while the opposite effect is observed for increasingly concentrated suspensions. Finally, the increase in L at rupture with increasing viscosity in the liquid case is opposite the reduction in thread length at rupture with increasing particle concentration, seen especially in the larger orifice.

3.3. A model for thread thinning

In order to quantify the effect of the added resistance, relative to the pure suspending liquid, of the suspensions to the thinning of the neck, we fit the evolution of R/a of both pure liquid and suspensions to the same mathematical form over a portion of the necking process. Recalling our earlier proposition that necking occurs in two separate stages for concentrated suspensions, we seek to determine whether the first stage of this process can be described simply in terms of an effective viscosity treatment of the suspensions.

The thinning data for the thread has been fitted to

$$R(t)/a = A(1 - e^{-B(t_0 - t)}) + C, \tag{1}$$

where $A > 0$ is the value of R/a away from pinching, $C < 0$ is a constant required since the value of R/a reaches zero before $t_0 - t = 0$ (owing to limitations of the detection algorithm), and B describes the rate of thinning of the thread radius during necking. This form for $R(t)/a$ was motivated by the work of Clanet and Lasheras (1999), who used a similar equation to describe the thread thinning rate in the process of forming drops of water as a function of orifice diameter.

3.3.1. R/a of pure liquids

The R/a data for the pure liquid mixtures of varying viscosity were fitted to (1). These fits are shown in Fig. 8c and d and the fitting parameters are presented in Table 2. The fits to (1) are good (the minimum adjusted R^2 value for the data regression to the fit equation was 0.996) as long as times "near" pinching are excluded; the times excluded, $(t_0 - t)_{(\min)}$, are evident from the fits and are also included in Table 2. The exponential decay form is not expected to describe the dynamics near thread rupture as noted by Clanet and Lasheras (1999).

The coefficient B of the exponential term in (1) provides a measure of the rate of the thread thinning during the first stage of necking and thus reflects the influence of viscosity, or mixture effective viscosity in the case of suspensions. As viscosity increases, the value of B decreases.

3.3.2. R/a of the suspensions

The averaged R/a data for the suspensions studied were also fitted to (1) and for all the suspensions the fit was found to be good. Examples of the fits, for $\phi = 0.05$ and 0.30 with $d = 0.16$ cm, are shown in Fig. 9 and for $\phi = 0.05$ and 0.40 with $d = 0.32$ cm in Fig. 10. The various fitting parameters for the suspensions are presented in Table 3.

As discussed briefly in the previous section the exponential coefficient B in (1) provides a measure of thinning rate for the time domain considered. For the suspensions, this rate is observed to decrease with increasing concentration (Table 3) for each orifice and particle size examined, indicating that the effective viscosity contribution due to the particle phase causes the observed changes in the thinning rate during the first stage of necking.

To gain insight to the manner in which changes in the thinning rate, B, are influenced by ϕ, the measured values of the thinning rate are plotted against an empirical effective viscosity of the suspensions (Fig. 11). The effective viscosity, μ_{eff}, is determined according to the Krieger (1972) viscosity formula

$$\mu_{\text{eff}}(\phi) = \mu(1 - \phi/\phi_{\max})^{-1.82}, \tag{2}$$

Table 2
Fitting parameters for Eq. (1) for the pure liquid mixtures

d (cm)	UCON (%)	μ (cP)	A	B (1/s)	C	$(t_0 - t)_{(\min)}$	R^2
0.16	30	310	18.4	38.4	−5.1	0.02	0.999
0.16	35	520	21.5	31.0	−8.4	0.03	0.998
0.16	40	870	25.1	25.0	−12.0	0.04	0.999
0.32	30	310	19.1	20.0	−7.4	0.04	0.997
0.32	35	520	21.5	17.0	−9.5	0.05	0.996
0.32	40	870	24.7	14.1	−13.2	0.08	0.996

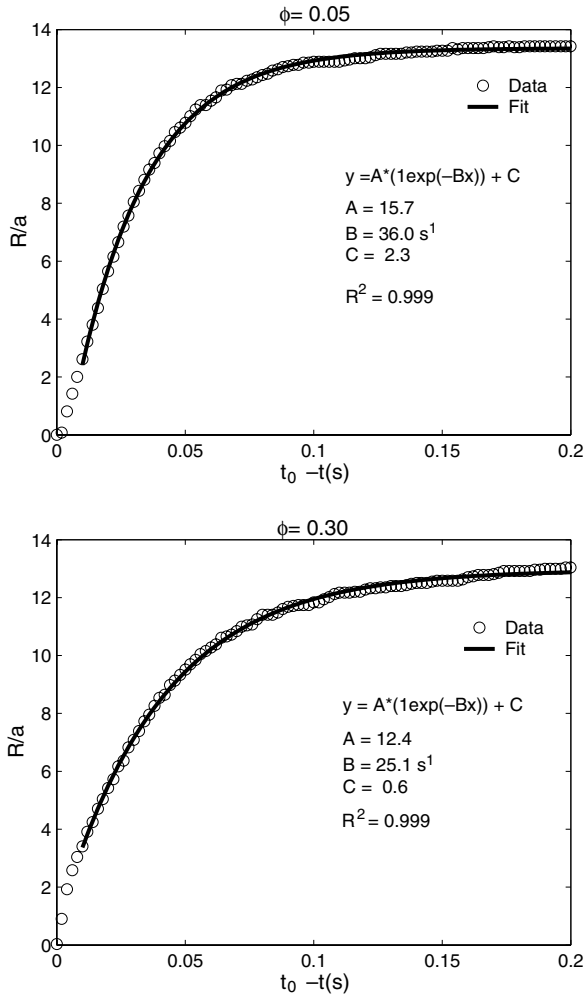

Fig. 9. An example of the fitted R/a data for $\phi = 0.05$ and 0.30, $d = 0.16$ cm, $d_p = 106$–125 μm.

with $\phi_{max} = 0.64$, the maximum packing particle fraction. The values of B for the various viscosity pure liquids are also plotted.

In Fig. 11a, the measured values of the thinning rate for the suspensions follow the same trend with increasing viscosity as that for the pure liquid mixtures for both of the orifices examined. Use of an effective viscosity in predicting the thinning rate during the early stage of necking is apparently warranted; note that the Krieger form proves satisfactory for describing this predominantly extensional motion despite being obtained from shearing data.

The thinning rate, represented by B, for both pure liquids and the suspensions is observed to be dependent upon the orifice diameter, the liquid properties, and the particle fraction. In these experiments the only liquid property which varies is the viscosity since the surface tension of the different pure liquid mixtures is essentially the same for all liquids used. The viscosity is varied either by changing the components in the cases of the different pure liquids, or by adding particles and changing the effective viscosity. Thus B is, in these experiments, a function only of the orifice diameter, d, and the mixture viscosity. From the data for the pure liquids it appears that $B \propto d^{-1}$ implying the quantity Bd is a constant for a given mixture, or within our study dependent only on viscosity. Fig. 11b shows the quantity Bd as a function of μ or μ_{eff}. The pure liquid data (the open circles in Fig. 11b) represent the average of the Bd values for both orifices and the error bars show the standard deviation. The solid line on the log–log plot has slope $-1/3$ and represents the data for the pure liquids and the

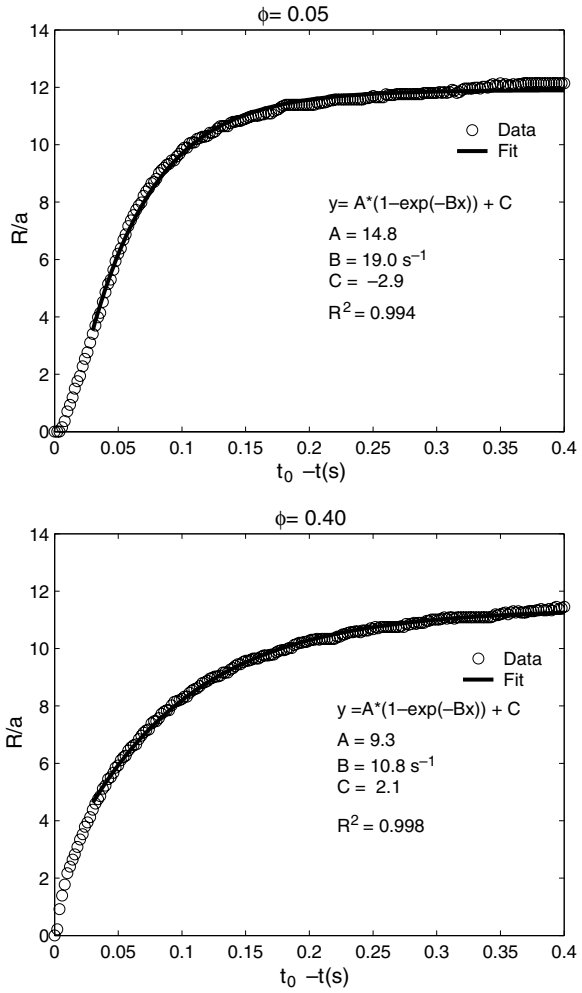

Fig. 10. An example of the fitted R/a data for $\phi = 0.05$ and 0.40, $d = 0.32$ cm, $d_p = 212$–250 μm.

Table 3
Fitting parameters for Eq. (1) for the suspensions

d (cm)	d_p (μm)	ϕ	A	B (1/s)	C	R^2
0.16	106–125	0.05	15.7	36.0	−2.3	0.999
0.16	106–125	0.10	14.5	34.6	−1.5	0.999
0.16	106–125	0.20	14.0	32.3	−0.8	0.999
0.16	106–125	0.30	12.4	25.1	0.6	0.999
0.32	212–250	0.05	14.8	19.0	−2.9	0.994
0.32	212–250	0.10	13.7	18.1	−1.5	0.994
0.32	212–250	0.20	12.5	17.5	−0.5	0.995
0.32	212–250	0.30	10.6	14.7	1.2	0.997
0.32	212–250	0.40	9.3	10.8	2.1	0.998
0.32	106–125	0.10	26.5	17.9	−2.7	0.993
0.32	106–125	0.20	24.8	17.9	−0.7	0.995
0.32	106–125	0.30	23.0	13.1	0.2	0.998
0.32	106–125	0.40	21.2	11.5	2.0	0.999

suspensions well, with the exception of the data for the $\phi = 0.20$ suspension which is uniformly above the line. Note, however, that the range of the data is relatively small.

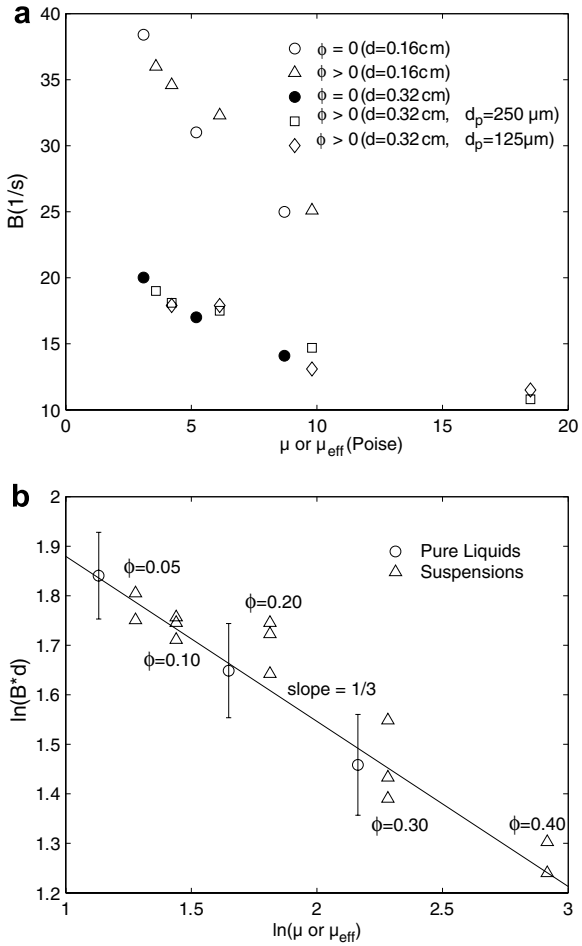

Fig. 11. Dependence of thinning rate, represented by B in (1), on viscosity. In (a) the measured values of B for all of the suspensions and pure liquids examined are presented as a function of either the pure liquid viscosity, μ, or the effective viscosity, μ_{eff}. In (b) the quantity $B * d$ is plotted against viscosity on a log–log scale.

3.4. Particle-induced fluctuations

In the previous sections, fluctuations induced by the presence of the particles illustrated by increased variability of L/d and R/a at finite ϕ have been noted. Here we investigate and quantify these fluctuations in the drop formation process, with our goals being to provide a more complete picture of the two-stage necking model proposed and to develop a technique for identifying the transition between the two stages. The ability to fit the necking data at times away from pinch-off to a form used for pure liquids supports this idea. Since the fits are only possible for times above a certain $t_0 - t$, the time at which the fit begins to deteriorate might be used as a lower bound for the times which encompass the first stage of necking. We develop here another technique involving determining the time at which a measure of the fluctuations begins to grow.

3.4.1. Average shape of forming drops

To develop a quantitative measure of the particle-induced fluctuations, the shapes of forming drops for a number of different experiments are averaged as a function of time prior to thread rupture. Early in the process, the fluctuations are generally observed to be small, but at pinch-off the fluctuations are large and lead to the very different structures observed for identical bulk conditions (*i.e.* at a fixed ϕ, d, d_{p}). This is illustrated in Fig. 12 which presents the pinch-off structures for five drop formation events from a suspension of $\phi = 0.20$

with $d = 0.32$ cm and $d_p = 212$–250 μm. We seek to identify when the fluctuations begin to grow and become "significant," with the idea that this time may signify the transition from stage-one to stage-two necking. Alternatively, one may view this approach as seeking to define a lower limit on the time from rupture for which drop shape is well-described by an average, or effective medium, approach, without reference to fluctuations induced by finite-sized suspended particles.

The first step was to average the shape leading up to rupture over several drop-forming events at each condition. The deviation from the mean is then determined. The shapes for a suspension of $\phi = 0.10$ at times approaching pinch-off are shown in Fig. 13 and will be used to illustrate implementation of the averaging scheme. The different curves represent the detected edge of the forming drop for five different experiments at the same conditions. The image resolution of the data in Fig. 13 was that of a single pixel, corresponding to 0.05 mm (50 μm), or $R/a = 0.376$ and $z/d = 0.006$. At early times, as seen in the uppermost plot at $t_0 - t \geqslant 0.10$ s, there is little or no deviation: the shapes of the forming drops are indistinguishable. As thinning continues, however, the curves begin to separate ($t_0 - t = 0.05$ s) with the axial deviation the most pronounced; note that at $t_0 - t = 0.01$ s, the minimum radius of the several drops remains similar. Finally, as rupture is approached, this axial spreading in length from drop to drop continues to increase and eventually radial fluctuations also grow rapidly in isolated locations. In attempting to average these shapes at a given time, the procedure was to take the mean of the various curves at each axial position. The axial variation in the curves introduced some difficulty in the averaging procedure, because near the end of the forming drop this averaging technique yields unrealistic values due to the large slopes (*i.e.*, variation of R with axial position). This problem could be alleviated through the use of a more sophisticated averaging technique, for example by considering the spread in the direction normal to the mean curve. However, the primary goal of this endeavor is to develop a measure of the difference between the curves and we use the deviation in L as the measure of difference of the shapes.

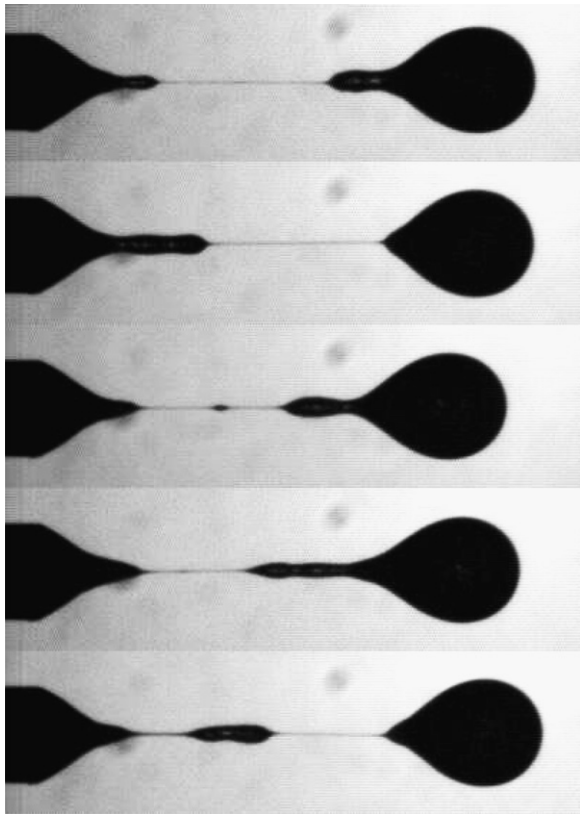

Fig. 12. Pinch-off structures for five different experiments for $\phi = 0.20$, $d = 0.32$ cm, $d_p = 212$–250 μm.

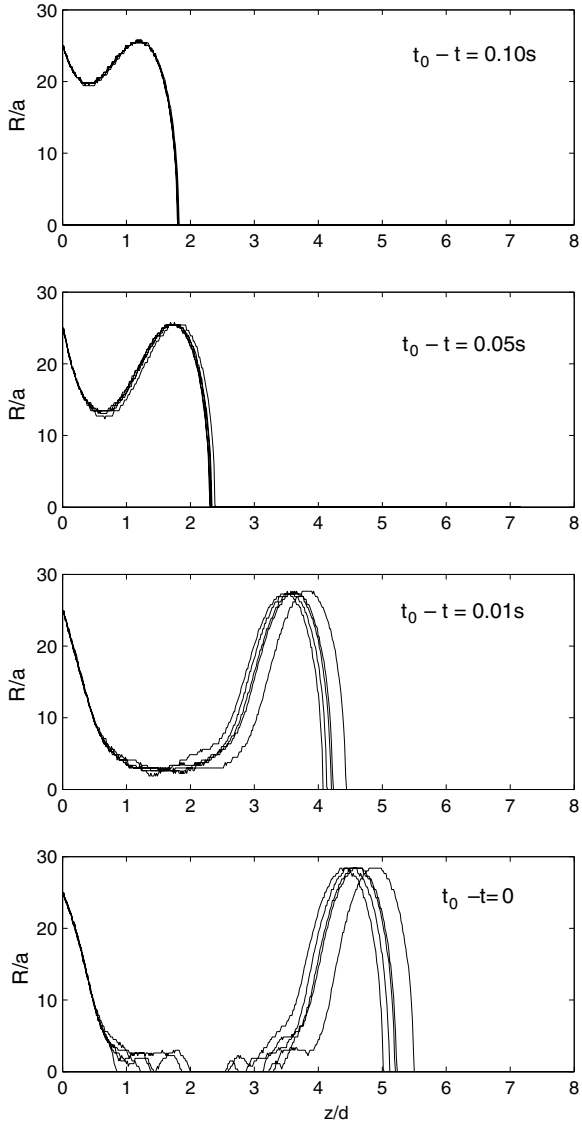

Fig. 13. Shapes for the forming drop at various times before and at thread rupture (at $t_0 - t = 0$) for $\phi = 0.10$, $d = 0.32$ cm, $d_p = 106$–125 μm.

3.4.2. Deviation in L

The fluctuations were found to appear first in L. The variability in the shapes of our sampling of $L(t)$ curves is thus represented here by the instantaneous standard deviation, $\Delta L(t)$. Results of this analysis are presented in Fig. 14. For each condition, ΔL is plotted as a function of time away from pinch-off, $t_0 - t$, with ΔL scaled arbitrarily by the mean particle diameter in the suspension used.

Fig. 14a presents $\Delta L(t)$ for the smaller orifice, $d = 0.16$ cm, with particles $d_p = 106$–125 μm ($d/d_p = 12.8$); ΔL values for the pure liquid and the $\phi = 0.05$ and 0.10 suspensions are very similar with significant growth in the standard deviation beginning at $t_0 - t \approx 0.05$ s and increasing to $\Delta L/d_p \approx 1.3$ just prior to pinch-off. For the two highest concentrations, $\phi = 0.20$ and 0.30, growth of the deviation occurs farther from rupture, at $t_0 - t \approx 0.07$ s, and the corresponding $\Delta L/d_p$ values at pinch-off are nearly twice as large. Note that the maximum deviation at pinch-off occurs for $\phi = 0.20$, and not for the most concentrated suspension examined in this set. The finding of an intermediate ϕ resulting in the greatest ΔL at pinch holds for the other orifice.

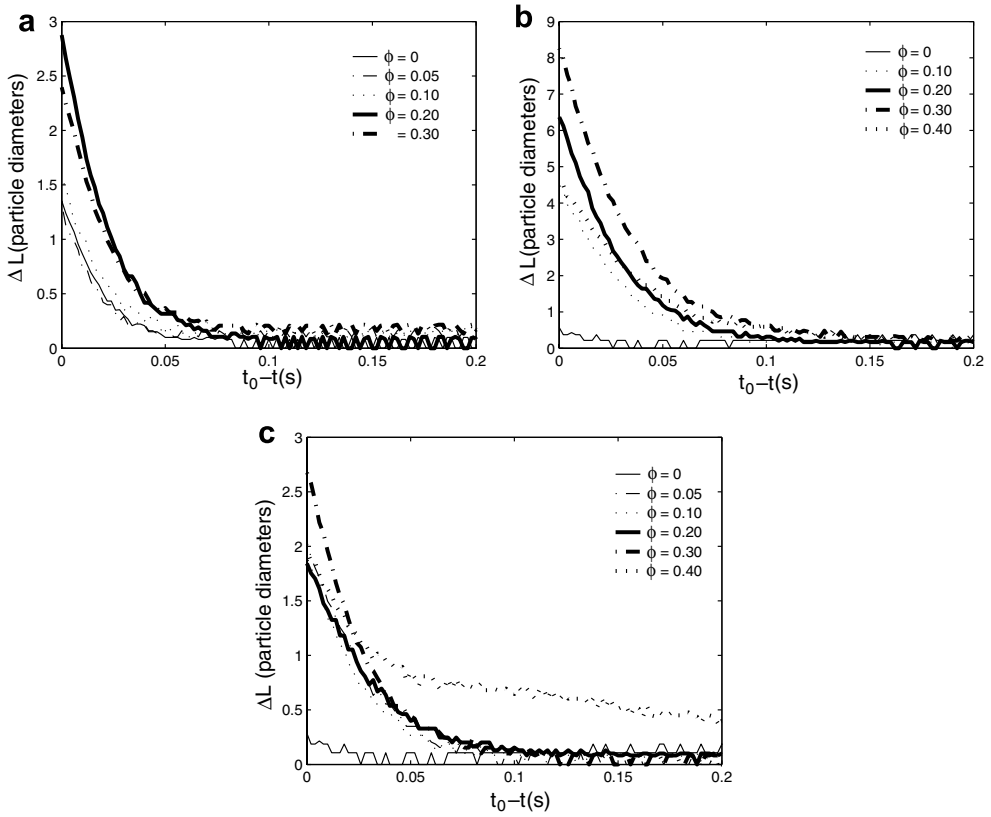

Fig. 14. Deviation in L for (a) $d = 0.16$ cm, $d_p = 106$–125 μm, (b) $d = 0.32$ cm, $d_p = 106$–125 μm, and (c) $d = 0.32$ cm, $d_p = 212$–250 μm.

Deviations at times well away from pinch-off are small and show no trend with time, and thus appear to characterize the noise in the experimental system, with the highest ϕ exhibiting slightly larger ΔL.

The length deviation for the larger orifice, $d = 0.32$ cm, with the smaller particles, $d_p = 106$–125 μm ($d/d_p = 25.6$), is shown in Fig. 14b. In this case, ΔL for the pure liquid remains small throughout the process (recall its growth near rupture for the small orifice) while the suspensions of all ϕ show a pronounced growth as rupture is approached. In this case the lowest-ϕ suspension, $\phi = 0.10$, has a rupture deviation of $\Delta L/d_p \approx 4.5$. The differing behavior of the pure liquids in the two orifices with respect to this measure may result from the stronger action of surface tension at the contact line of the smaller orifice, perhaps magnifying small surface imperfections in the capillary or changes in the wetting from drop to drop. The ΔL behavior for the small-particle suspensions ($d/d_p = 25.6$) through the larger orifice is similar to that described for the smaller orifice ($d/d_p = 12.8$). The standard deviation increases with ϕ until $\phi = 0.30$ and then decreases quite markedly for the highest-ϕ suspension ($\phi = 0.40$). The values of $\Delta L/d_p$ are 2–3 times larger than those for the corresponding suspensions in the smaller orifice, suggesting that the ratio d/d_p is relevant in understanding the fluctuations. The times when the deviations start to increase are slightly greater than those observed for the smaller orifice; the flow rate for the larger orifice is twice that for the smaller orifice ($Q = 0.5$ and 0.25 cm^3/min, respectively). It is not possible to state precisely when the fluctuations begin to become significant but it occurs in the range of $t_0 - t$ of 0.07–0.1 s with increasing ϕ leading to earlier fluctuations.

Fig. 14c presents the data for the ΔL fluctuations for the larger orifice, $d = 0.32$ cm, with the larger particles, $d_p = 212$–250 μm, and hence with $d/d_p = 12.8$ of the same value as in the results of Fig. 14a. We observe some strikingly different behavior from either of the other two cases at the highest particle concentration. The low-ϕ suspensions exhibit similar behavior to that of the smaller orifice with $\Delta L/d_p$ of similar magnitude (in this case directly comparable since d/d_p is the same) and begin to grow at $t_0 - t \approx 0.07$ s; one might expect a need to rescale time, but this may be largely captured by the proportional increase in Q with d. The notable

difference in behavior occurs for the $\phi = 0.40$ suspension. In this case $\Delta L/d_p$ is much larger than that of the lower-ϕ suspensions at times far from pinch-off. This behavior is seen only for the largest ϕ and smaller d/d_p studied; $\phi = 0.4$ at the larger d/d_p (smaller particles) exhibits very small ΔL far from the rupture time. This suggests that suspensions of elevated ϕ develop correlations in their structure leading to fluctuations in effective properties which are sampled by the smaller d/d_p but not the larger.

4. Discussion and concluding remarks

The goal of this study of the evolution of forming drops, in particular the dynamics of the stretching and thinning of the thread, has been to develop detailed understanding of particulate effects on the drop formation process. Specifically, we have focused on investigating the proposition (Furbank and Morris, 2004) that the drop formation for concentrated suspensions can be thought of as occurring according to a two-stage process. Here, we discuss the experimental results further, probe the validity of the two-stage necking model, and present the conclusions we have drawn.

4.1. Particle effects on thread dynamics

The primary particulate effects on the thread dynamics are observed to be an added resistance to thinning of the thread, and a reduction in thread length at rupture. These two effects both result at a most basic level from the rigidity of the particles, but otherwise may be viewed as having quite separate origins. The resistance to thinning of the thread can be seen as an effective continuum effect, *i.e.* one captured well by effective viscosity, while the tendency toward shorter length at rupture caused by the particles is an effect of the discrete nature of the particles.

For more viscous pure liquids, the slowing of thinning continues throughout the necking process even up to rupture. In sharp contrast, the effective viscosity effect of slowing the thinning rate as ϕ increases is reversed for times near pinch-off: here, we observe the rate of thinning to increase sharply with ϕ. We recall that the thread has thinned to as small as ~4–5 particle diameters by this point in the process so the thread can be visualized as essentially a cylinder of liquid with a small number of particles spanning its cross-section. The fluctuations in properties apparently become rather extreme, and at these times the particles must be considered discrete solid bodies and their unique arrangement within the thread dictates how necking proceeds. For the thread to rupture, the particles must be rearranged such that a particle-free region develops over which final necking occurs. Thus the final necking toward rupture occurs over an axially localized portion of the thread, a zone with much lower ability to resist deformation than the mean material, and this localization which occurs as the stretching transitions from thinning over a particle-rich to a particle-free region leads to much steeper slopes in the R/a curves at elevated ϕ. This process has, at least phenomenologically, some analogy with the necking and rupture observed in solid material testing (for example, see Rao and Mohan, 2001).

The appearance of an additional length scale—d_p in addition to d—is found to be related to the steepening of the R/a curve near pinch-off and the reduced length of the thread at rupture. For pure liquids there is no length scale deriving from the apparatus other than the orifice diameter, and the final necking is governed by the viscous length scale, L_μ, a quantity derived solely from the liquid properties. This viscous length scale, as proposed by Peregrine et al. (1990), is defined as

$$L_\mu = \frac{\mu^2}{\rho\sigma} \tag{3}$$

This length scale is used in determining the range over which similarity solutions are possible for the shape of the forming drop. In our experiments $L_\mu = 1.7$ mm for the suspending liquid, and larger for the other liquids studied. This suggests applicability of the work of numerous researchers modeling the dynamics of the thread at times very near pinch-off (Eggers and Dupont, 1994; Shi et al., 1994) although in the case of concentrated suspensions this technique does not appear to be applicable for two reasons. The first is the pinch-off structure itself, which has been shown to have wide variability as pinch-off is approached, with the size and shape of the spindles fluctuating from drop to drop. The other is the presence of the particles introducing a new length scale

to the problem. Pure liquid results may be useful for determining the thinning rate of the liquid thread after a particle-free region has developed, but the scales involved ultimately drop below the level of detection in this work. The experimental evidence supports the assertion that addition of finite-sized particles is responsible for the decrease in the pinch-off length of the suspensions relative to the pure liquid. This effect is not attributable to the modification of the bulk viscosity of the mixture, as higher-viscosity pure liquids attain much longer thread lengths than the lower viscosity suspending liquid.

The particles also increase the variability in the process, with the standard deviation in connected length, $\Delta L(t)$, used here as a measure of the particle-induced fluctuations. One feature of note in these measurements is the time at which the fluctuations start to increase. From the analysis of the thinning data we found that data from times fairly close to pinch-off ($t_0 - t \approx 0.03$ s) was fitted well by the model used for the pure liquid suggesting fluctuations up to this time should be minimal. However, for each of the orifice diameters and particle sizes examined, ΔL begins to increase visibly at $t_0 - t \approx 0.07$–0.08 s. Another result from the particle fluctuation analysis is the presence of an intermediate particle concentration for which the fluctuations are maximized. For each orifice this concentration corresponds to the next to highest ϕ investigated ($\phi = 0.20$ for $d = 0.16$ cm and $\phi = 0.30$ for $d = 0.32$ cm). This indicates that increasing ϕ can actually have a stabilizing effect on the process, as discussed previously (Furbank and Morris, 2004) in relation to the reduced number of satellite drops observed at elevated ϕ.

4.2. Validity of two-stage model

A two-stage necking model for drop formation from suspensions (Furbank and Morris, 2004) is based on the idea that initial and final necking involve the transition from a regime where particulate effects on the thread dynamics are governed by bulk properties to one where discrete particle (finite-size) effects dominate. According to this description, the particle effects in the first stage can be attributed solely to a change in bulk properties, and we have found this to be simply an increase of the effective viscosity, of the mixture. In the second stage, the width of the thread has thinned sufficiently that a continuum description of the material is no longer possible. At this point the discreteness of the particles and the individual particle motions within the collapsing thread are responsible for the very different pinch-off structures observed for the suspensions.

The initial necking stage of the two-step process has been investigated using the model presented in Section 3.3 for the decay of the thread radius, with fits of the data indicating that the early necking stage of the drop formation is well described by this model developed for pure liquids. Using this technique we found that the thinning rate for pure liquids or suspensions scales linearly with the orifice diameter as in earlier work (Clanet and Lasheras, 1999), and with viscosity to the $-1/3$ power. We conclude that during initial necking the primary particulate effect is, in fact, to add to the effective viscosity of the mixture. The particle size effect on the process during initial necking is, for most conditions studied here, negligible until d/d_p becomes small enough that a continuum description of the material in the forming drop is no longer reliable. We recall, however, that for $d/d_p = 12.8$ and $\phi = 0.4$, the fluctuations in axial length were much stronger than for the same particle fraction and a larger d/d_p; hence the minimum relative length scale is ϕ-dependent.

Implicit in the proposition that the necking process of suspensions is described by a two-stage model is the need to identify the transition between the two stages. In this, we have not achieved an unambiguous result. We have treated our experimental data in a number of ways not reported in detail here, including shifting the time considered as the rupture time—an example which seems plausible but is arbitrary because the time when our detection method is no longer able to detect a finite radius of thread—and can report no success in collapsing the R/a curves. Based on the argument that the transition accompanies the change in the dominant length scale in the problem from the orifice diameter to the particle diameter, the transition should be a function of R/a. Using the minimum time away from pinch-off above which the fits were possible we were able to determine the thickness of the thread at this time for the various suspensions. These times and R/a values are presented in Table 4. From the average values for a given d and d_p combination, it appears that the transition between the two stages using this technique is dependent on the ratio of the capillary to particle diameter, d/d_p. This is supported by the similar values for the two different orifices with the same d/d_p ($R/a \sim 3$–4). However, values for different d_p through the larger orifice have the same absolute half-width (R) at transition, suggesting that particle size is a weak factor (we would expect the thickness of the thread at the transition between the

Table 4
Thread thickness at the minimum time used in fitting the R/a data

ϕ	d (cm)	d_p (μm)	$t_0 - t$ (s)	R/a
0.05	0.16	106–125	0.01	2.6
0.10	0.16	106–125	0.01	2.9
0.20	0.16	106–125	0.01	3.2
0.30	0.16	106–125	0.01	3.4
Average				3.0
0.05	0.32	212–250	0.03	4.0
0.10	0.32	212–250	0.03	3.8
0.20	0.32	212–250	0.03	4.3
0.30	0.32	212–250	0.03	4.7
0.40	0.32	212–250	0.03	4.4
Average				4.2
0.10	0.32	106–125	0.03	7.9
0.20	0.32	106–125	0.03	8.9
0.30	0.32	106–125	0.03	7.5
0.40	0.32	106–125	0.03	8.0
Average				8.1

stages to be smaller for the smaller particles). We conclude that the two-stage model has utility in simplifying and focusing analysis, but is ambiguous in that there is no clear point of transition between the two stages. It is worthy of note that a range of engineering issues such as drop size are controlled by the first stage, and thus can be described by a fairly simple effective fluid approach in the pendant drop case. Whether this remains true in rapid drop formation, as in drop-on-demand devices, is a topic for further study.

Acknowledgement

This work was supported in part by NASA Microgravity Fluid Physics (NAG3-2739) and also by the National Textile Center (C99-GT07).

References

Ambravaneswaran, B., Wilkes, E.D., Basaran, O.A., 2002. Drop formation from a capillary tube: comparison of one-dimensional and two-dimensional analyses and occurrence of satellite drops. Phys. Fluids 14, 2606–2621.

Chen, A.U., Notz, P.K., Basaran, O.A., 2002. Computational and experimental analysis of pinch-off and scaling. Phys. Rev. Lett. 88, 1–4.

Clanet, C., Lasheras, J.C., 1999. Transition from dripping to jetting. J. Fluid Mech. 383, 307–326.

Eggers, J., 1997. Nonlinear dynamics and breakup of free-surface flows. Rev. Mod. Phys. 69, 865–929.

Eggers, J., Dupont, T.F., 1994. Drop formation in a one-dimensional approximation of the Navier–Stokes equation. J. Fluid Mech. 262, 205–221.

Furbank, R.J., Morris, J.F., 2004. An experimental study of particle effects on drop formation. Phys. Fluids 16, 1777–1790.

Krieger, I.M., 1972. Rheology of monodisperse lattices. Adv. Colloid Interface Sci. 3, 111–136.

Peregrine, D.H., Shoker, G., Symon, A., 1990. The bifurcation of liquid bridges. J. Fluid Mech. 212, 25–39.

Rao, K.P., Mohan, E.V.R., 2001. A unified test for evaluating material parameters for use in modelling of sheet metal forming. J. Mater. Process. Technol. 113, 725731.

Shi, X.D., Brenner, M.P., Nagel, S.R., 1994. A cascade of structure in a drop falling from a faucet. Science 265, 219–222.

Wilkes, E.D., Phillips, S.D., Basaran, O.A., 1999. Computational and experimental analysis of dynamics of drop formation. Phys. Fluids 11, 3577–3598.

Zhang, X., Basaran, O.A., 1995. An experimental study of dynamics of drop formation. Phys. Fluids 7, 1184–1203.